Article

Journal of the Brazilian Chemical Society

https://dx.doi.org/10.21577/0103-5053.20240224

J. Braz. Chem. Soc. **2025**, *36*, 4, e-20240224, 1-12

Acridone Derivatives as Photosystem II Inhibitors: Synthesis, Herbicidal Activity, and Structure-Activity

Jessica Maria de Souza,[a] Paulo S. Medeiros,[a] Taciane S. Pitteri,[a] Mariana A. Silva,[a] Marcelo Augusto F. Basso,[a] Leonardo G. de Vasconcelos,[a] Evandro Luiz Dall'Óglio,[a] Olívia M. Sampaio[a] and Lucas C. C. Vieira[*,a]

[a]Departamento de Química, Universidade Federal de Mato Grosso, 78060-900 Cuiabá-MT, Brazil

In this study, we report the synthesis of acridone derivatives and their potential as photosystem II (PSII) inhibitors, as well as their pre- and post-emergence herbicidal activities through chlorophyll a fluorescence and germination assays. Among the compounds tested for PSII activity, acridin-9(10*H*)-one showed the most promising results, reducing the performance index on an absorption basis and decreasing the quantum yield for electron transport compared to the control. These findings suggest an inhibitory effect on PSII within the electron transport chain. Additionally, 2-chloroacridin-9(10*H*)-one and 9(10*H*)-acridone-4-carboxylic acid exhibited post-emergence herbicidal activity against *Amaranthus lividus* and *Amaranthus viridis* weeds, respectively, leading to a reduction in radicle and hypocotyl lengths. Furthermore, we applied a molecular docking approach with the D1 protein and 4-hydroxyphenylpyruvate dioxygenase to investigate the structure-activity relationships among the acridone derivatives with these enzymes. The analysis highlighted the importance of the carbonyl group and aromatic substituents on the acridone scaffold facilitating ligand interactions, especially through hydrogen bonding. Consequently, our research group aims to optimize these molecular features to develop new, potent bioactive molecular scaffolds.

Keywords: acridone, D1 protein, herbicide, molecular docking, photosynthesis

Introduction

Acridones are a diverse and versatile class of alkaloids that can be obtained from natural sources or synthesized through various methodologies, yielding compounds with unique molecular features.[1] This structural versatility has enabled the development of a wide range of acridone derivatives that exhibit significant biological activities, including antiparasitic,[2] antimicrobial,[3] anti-inflammatory,[4] antioxidant,[5] and phytotoxic effects.[6] Numerous *N*-heterocyclic compounds have been investigated for their herbicidal potential, such as carbazoles,[7] indoles,[8] quinolines,[9] quinolizidines,[10] and quinazoline-2,4-diones.[11] For example, compounds like γ-fagarine (**1**),[12] a chlorinated carbazole derivative (**2**),[13] 3,5-diacetyl-1,4-dihydrolutidine (**3**),[14] indole (**4**),[15] and quinolone (**5**)[16] have demonstrated phytotoxic activity by blocking the photosynthetic electron transport chain (Figure 1).

Limited research on the phytotoxicity properties of acridones derivatives highlights the potential for further exploration in this field. Although some acridone derivatives, such as citrusinine-I and glycocitrine-IV, have

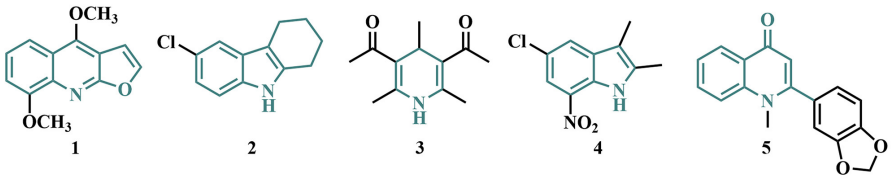

Figure 1. *N*-Heterocyclic compounds that act as photosynthesis inhibitors.

*e-mail: lucas.vieira@ufmt.br
Editor handled this article: Albertina Moglioni (Associate)

shown inhibitory activity of the photosystem II (PSII) electron transport chain,[17] their specific modes of action and herbicidal efficacy remain largely unexplored. Similarly, graveoline has exhibited both pre- and post-emergence herbicidal activity against the weed *Lepidium sativum*, suggesting the potential of acridone derivatives as herbicidal agents.[6] In this context, the synthesis and evaluation of acridone derivatives for herbicidal activity represents an emerging area of research that could lead to the development of new classes of weed control agents.

Molecular docking has been employed to understand the chemical interactions involved in PSII electron chain inhibition and to elucidate key biochemical processes related to germination and plant growth inhibition.[18] The D1 protein of PSII has been particularly useful for predicting chemical interactions at the quinone B binding site with small molecules. Notable examples include brassicanate A sulfoxide, recognized for its strong phytotoxic effects against *Lactuca sativa* Linn., *Panicum miliaceum*, and *Chenopodium album* weeds,[19] fluorinated chalcones with pre- and post-emergent herbicidal activity against *Amaranthus* weeds,[20] and cytochalasin A, a mycotoxin that induces leaf lesions on *Ageratina adenophora*.[21]

The 4-hydroxyphenylpyruvate dioxygenase (HPPD) protein is a key target in herbicide research due to its critical role in plant development.[22] Molecular docking studies on HPPD have yielded valuable insights into the structure-activity relationships of compounds with herbicidal potential. For instance, piperidinone derivatives have demonstrated herbicidal activity against weeds such as *Echinochloa crus-galli*, *Abutilon theophrasti*, and *Setaria viridis*.[23] Similarly, triketone compounds with a quinoxaline scaffold have shown potent inhibition of *Arabidopsis thaliana* HPPD.[24] Additionally, pyrazole aromatic ketones have exhibited phytotoxic activity against weeds like *Chenopodium serotinum*, *Stellaria media*, and *Brassica juncea*.[25] These findings highlight the importance of molecular docking in elucidating herbicidal mechanisms and supporting the development of effective herbicidal agents.

Based on this context, the aims of the current work were to synthesize acridone derivatives with different substituent groups and to evaluate their effects on the photosynthetic apparatus and plant development. This evaluation involved radicle and hypocotyl growth assays, along with molecular docking studies.

Experimental

General information

All commercially available reagents and solvents were used without further purification. Reaction progress was monitored by thin-layer chromatography on silica gel 60 UV254 pre-coated plates with a thickness of 0.20 mm (Macherey-Nagel, Düren, Germany), with detection via ultraviolet lamp. Flash column chromatography was conducted on 230-400 mesh silica gel (Merk, Germany). Nuclear magnetic resonance (NMR) of ^{1}H and ^{13}C spectra were recorded using a Bruker Magnet System AscendTM spectrometer (Bruker, Switzerland), operating at 500 and 125 MHz for ^{1}H and ^{13}C, respectively. Chemical shifts were reported relative to the internal standard tetramethylsilane (δ 0.00 ppm) for ^{1}H NMR spectroscopy, with deuterated dimethyl sulfoxide (DMSO-d_6) and deuterated chloroform (Cambridge Isotope Laboratories, USA) as solvents. Fourier transform infrared spectroscopy (FTIR) spectra were obtained using a Shimadzu Iraffinity-1 spectrophotometer (Japan, Shimadzu) in potassium bromide pellets (Spectrum, USA).

Synthesis of 2-iodobenzoic acid (**7**)

Following a modified procedure,[26] a solution of sodium nitrite (1.59 g, 23.0 mmol in 10.0 mL of water) was gradually added to a flask containing 2-aminobenzoic acid (**6**) (22.0 mmol, 3.0 g) and 37% hydrochloric acid (20.0 mL) at 0 ºC. The reaction mixture was then stirred vigorously for 10 min. An aqueous solution of potassium iodide (9.0 g, 54.0 mmol in 7.0 mL of water) was added, and the mixture was left to stir for 1 h. The reaction mixture was subsequently treated with a 10% aqueous solution of sodium sulfite (15.0 mL). The resulting solid was filtered under reduced pressure, dried, and further purified by recrystallization from hot water, yielding pure 2-iodobenzoic acid with a 61% yield (3.0 g) chemical yield. ^{1}H NMR (500 MHz, DMSO-d_6) δ 7.24 (ddd, 1H, *J* 1.6, 1.7, 7.5 Hz), 7.48 (ddd, 1H, *J* 0.9, 1.2, 7.5 Hz), 7.71 (dd, 1H, *J* 1.7, 7.7 Hz), 7.98 (dd, 1H, *J* 0.9, 7.9 Hz), 13.32 (br s, 1H); ^{13}C NMR (125 MHz, DMSO-d_6) δ 94.5, 128.6, 130.5, 132.9, 137.3, 140.9, 168.6.

Synthesis of 2-arylaminobenzoic acid derivatives (**9a-9e**)

Following the literature procedure,[27] a solution of compound **7** (2.4 mmol, 0.6 g), aniline derivatives (**8a-8e**) (45.0 mmol), copper powder (1.3 mmol, 82.5 mg), potassium carbonate (34.0 mmol, 4.7 g) in 15 mL of ethanol was refluxed for 17 h. After completion, the reaction mixture was cooled to room temperature, poured into hot water, and boiled with activated charcoal for 15 min. The mixture was then filtered through Celite, and the filtrate was acidified with HCl to precipitate the product. The

resulting precipitate was collected by filtration under reduced pressure, washed with water, and no additional purification was considered necessary.

2-(Phenylamino)benzoic acid (**9a**)[28]

White solid; yield: 59%; ^{1}H NMR (500 MHz, DMSO-d_6) δ 6.74 (t, 1H, *J* 7.7 Hz), 7.12 (t, 1H, *J* 7.32 Hz), 7.21 (d, 1H, *J* 8.3 Hz), 7.25 (d, 2H, *J* 7.4 Hz), 7.32-7.37 (m, 3H), 8.03 (dd, 1H, *J* 1.2, 8.0 Hz), 9.30 (s, 1H).

2-((4-Chlorophenyl)amino)benzoic acid (**9b**)[28]

Grey solid; yield: 61%; ^{1}H NMR (500 MHz, DMSO-d_6) δ 6.82 (t, 1H, *J* 7.8 Hz), 7.22-7.27 (m, 3H), 7.36-7.43 (m, 3H), 7.90 (dd, 1H, *J* 1.4, 8.0 Hz), 9.61 (s, 1H), 13.14 (s, 1H).

2-((4-Bromophenyl)amino)benzoic acid (**9c**)[29]

Grey solid; yield: 61%; ^{1}H NMR (500 MHz, DMSO-d_6) δ 6.84 (t, 1H, *J* 7.3 Hz), 7.20-7.27 (m, 3H), 7.41-7.44 (m, 1H), 7.49-7.53 (m, 2H), 7.91-7.96 (m, 1H), 9.61 (s, 1H), 13.14 (s, 1H).

2,2'-Dicarboxydiphenylamine (**9d**)[30]

White solid; yield: 80%; ^{1}H NMR (500 MHz, DMSO-d_6) δ 6.96 (ddd, 2H, *J* 1.4, 1.6, 8.0 Hz), 7.25 (d, 2H, *J* 7.4 Hz), 7.43-7.49 (m, 4H), 7.93 (dd, 2H, *J* 1.2, 7.7 Hz), 10.83 (s, 1H).

2-((4-Chloro-2-nitrophenyl)amino)benzoic acid (**9e**)[31]

Orange solid; yield: 90%; ^{1}H NMR (500 MHz, DMSO-d_6) δ 7.12 (t, 1H, *J* 7.2 Hz), 7.53-7.56 (m, 2H), 7.62-7.66 (m, 2H), 7.98 (d, 1H, *J* 7.4 Hz), 8.15-8.16 (m, 1H), 11.10 (s, 1H).

Synthesis of acridone derivatives (**10a-10e**)

Following a modified literature procedure,[27] a mixture of compounds **9a-9e** (0.41 mmol) and concentrated sulfuric acid (4.1 mmol) was heated at 100 °C for 3 h. Upon completion, the reaction mixture was poured into 20 mL of hot water. After cooling to room temperature, the reaction mixture was made alkaline by the dropwise addition of a saturated aqueous solution of sodium bicarbonate. The resulting precipitate was filtered under reduced pressure, washed with water, and no additional purification was considered necessary.

Acridin-9(10*H*)-one (**10a**)[32]

Yellow solid; yield: 53%; IR (KBr) ν / cm^{-1} 1190, 1469, 1591, 1643, 2989, 3111; ^{1}H NMR (500 MHz, DMSO-d_6) δ 7.24-7.27 (m, 2H), 7.55 (d, 2H, *J* 8.2 Hz), 7.73 (ddd, 2H, *J* 1.6, 6.8, 8.4 Hz), 8.23 (dd, 2H, *J* 1.3, 8.1 Hz), 11.75 (s, 1H); ^{13}C NMR (125 MHz, DMSO-d_6) δ 117.8, 120.9, 121.4, 126.4, 133.9, 141.3, 177.2.

2-Chloroacridin-9(10*H*)-one (**10b**)[33]

Yellow solid; yield: 60%; IR (KBr) ν / cm^{-1} 752, 1165, 1467, 1573, 1635, 2980, 3415; ^{1}H NMR (500 MHz, DMSO-d_6) δ 7.27-7.30 (m, 1H), 7.56 (d, 1H, *J* 8.2 Hz), 7.58 (d, 1H, *J* 8.9 Hz), 7.74-7.77 (m, 2H), 8.16 (d, 1H, *J* 2.5 Hz), 8.23 (dd, 1H, *J* 1.3, 8.0 Hz), 11.94 (s, 1H); ^{13}C NMR (125 MHz, DMSO-d_6) δ 118.0, 120.3, 120.7, 121.7, 122.0, 125.2, 125.8, 126.4, 133.9, 134.3, 139.9, 141.2, 176.2.

2-Bromoacridin-9(10*H*)-one (**10c**)[32]

Yellow solid; yield: 79%; IR (KBr) ν / cm^{-1} 754, 1165, 1463, 1525, 1710, 2972, 3444; ^{1}H NMR (500 MHz, DMSO-d_6) δ 7.52-7.56 (m, 2H), 7.74-7.78 (m, 1H), 7.85 (dd, 1H, *J* 2.4, 8.8 Hz), 8.21 (d, 1H, *J* 8.1 Hz), 8.29 (d, 1H, *J* 2.3 Hz), 11.93 (s, 1H); ^{13}C NMR (125 MHz, DMSO-d_6) δ 113.6, 118.0, 120.5, 120.8, 122.0, 122.2, 126.5, 128.4, 134.3, 136.4, 140.2, 141.2, 176.1.

9(10*H*)-Acridone-4-carboxylic acid (**10d**)[34]

Yellow solid; yield: 40%; IR (KBr) ν / cm^{-1} 748, 1230, 1523, 1598, 1687, 3061, 3211; ^{1}H NMR (500 MHz, DMSO-d_6) δ 7.32-7.37 (m, 2H), 7.77-7.79 (m, 2H), 8.23 (d, 1H, *J* 8.1 Hz), 8.44 (dd, 2H, *J* 1.7, 7.5 Hz), 8.53 (dd, 1H, *J* 1.4, 8.0 Hz), 11.96 (s, 1H), 13.0 (s, 1H); ^{13}C NMR (125 MHz, DMSO-d_6) δ 115.4, 119.1, 120.7, 121.1, 122.1, 122.8, 126.3, 132.9, 134.6, 137.4, 140.4, 141.7, 169.6, 177.0.

2-Chloro-4-nitroacridin-9(10*H*)-one (**10e**)[35]

Orange solid; yield: 73%; IR (KBr) ν / cm^{-1} 765, 1284, 1504, 1595, 1618, 3086, 3286; ^{1}H NMR (500 MHz, DMSO-d_6) δ 7.38-7.41 (m, 1H), 7.46 (d, 1H, *J* 8.2 Hz), 7.76 (ddd, 1H, *J* 1.4, 1.6, 8.4 Hz), 8.42 (d, 1H, *J* 8.0 Hz), 8.67 (d, 1H, *J* 2.6 Hz), 8.80 (d, 1H, *J* 2.5 Hz), 11.16 (s, 1H); ^{13}C NMR (125 MHz, DMSO-d_6) δ 117.9, 121.5, 124.1, 125.0, 125.8, 127.5, 131.2, 134.3, 134.7, 135.1, 135.8, 139.4, 175.8.

Chlorophyll a fluorescence measurement

Similar to our previous report,[36] spinach (*Spinacia oleracea*) leaves were cut into 1.0 cm diameter discs, with 10 discs placed in each 9 cm Petri dish containing 20 mL of Krebs solution. The Krebs solution included NaCl (115 mM), KCl (5.9 mM), $MgCl_2$ (1.2 mM), KH_2PO_4 (1.2 mM), Na_2SO_4 (1.2 mM), $CaCl_2$ (25 mM), and $NaHCO_3$ (25 mM), adjusted to pH 7.4. After a 12-h incubation under a photoperiod at 21 ºC, solutions of

compounds **10a-10e** in 1% dimethyl sulfoxide (DMSO) were added to each dish to achieve a concentration of 100 μM, with DMSO as the negative control. Following 6 h of incubation with the acridone derivatives, the discs were kept in darkness for 30 min before measuring chlorophyll a (Chl a) fluorescence using the Handy Plant Efficiency Analyzer (Hansatech Instruments Ltd., England).

Germination

Following a modified literature procedure,[37] twenty seeds each of *Amaranthus lividus* and *Amaranthus viridis* were placed in 9 cm Petri dishes containing filter paper. The dishes were then moistened with either 4 mL of sterile deionized water containing 1% DMSO (used as the negative control) or solutions of compounds **10a-10e** at a concentration of 100 μM. Each treatment included seven replicates. Seed germination was conducted under a day/night temperature cycle at 25 °C. To prevent moisture loss, the Petri dishes were sealed with paraffin film.

Daily germination counts were recorded, and cumulative germination was assessed after seven days. A seed was considered germinated when the radicle or hypocotyl reached a length of at least 2 mm. Germination percentage (GP) was calculated as the ratio of germinated seeds to the total number of seeds initially placed in each Petri dish. The germination index (GI) was calculated using the formula: $GI = \Sigma(Gi \times I)$, where Gi represents the number of seeds germinated on day I. The mean germination time (MGT) was determined using the formula: $MGT = \Sigma(Gi \times I)/\Sigma(I)$. Additionally, radicle (RL) and hypocotyl (HL) lengths of germinating seedlings were measured using a pachymeter. The seed vigor index (SVI) was calculated as SVI = seedling length × germination percentage.

Molecular docking

Docking studies were conducted to analyze the interactions of acridones **10a-10e** with two key proteins: the D1 protein of PSII and HPPD. The 3D crystal structures of the D1 protein (PDB ID: 4v82)[38] and HPPD (PDB ID: 6j63)[39] were obtained from the Protein Data Bank. Co-factors and water molecules were removed, and polar hydrogen atoms were added to the structures. Atom charges for both proteins were assigned using the Gasteiger method with AutoDockTools (ADT).[40]

The 3D structures of the acridone derivatives **10a-10e**, as well as the reference compounds terbutryn and nitisinone (NTBC), were generated using ChemDraw software.[41] Geometry optimizations were performed using the MM2 force field in ChemBio3D,[41] and the ligands were converted to pdbqt format for virtual screening with ADT.

Virtual screening was conducted using AutoDock Vina,[42] with protein structures converted to pdbqt format and configuration parameters specified in a config.txt file. During the docking process, AutoDock 4.2[43] was used, setting the grid box center at coordinates (40, 40, 40) for the x, y, and z axes with a grid spacing of 0.286 Å. This grid was centered on the active site of each target protein. For the D1 protein, the grid box was centered at x = 21.804, y = 67.331, and z = 34.939, while for HPPD, it was centered at x = 33.275, y = −19.839, and z = 5.061. Twenty independent runs were performed for each docking experiment.

The optimal docking orientations were determined based on key interacting residues, the number of hydrogen bonds, and binding energy. Intermolecular interactions between ligands and proteins were analyzed using BIOVIA Discovery Studio 2024,[44] and images were generated using PyMOL.[45]

Statistical analysis

To evaluate the effects of acridone derivatives **10a-10e** on Chl a fluorescence and germination parameters, we conducted a one-way analysis of variance (ANOVA). *Post-hoc* comparisons were performed using Tukey's test, with a significance set at $p \leq 0.05$. Levine's test was used to assess the homogeneity of variance, while data normality was checked as part of the analysis. All statistical analyses were carried out using GraphPad Prism.[46] Results were reported as the mean ± standard error of the mean (SEM).

Results and Discussion

Chemistry

A multistep approach was employed to synthetize the acridone derivatives (**10a-10e**). The first step involved preparing 2-iodobenzoic acid (**7**) via diazotization of 2-aminobenzoic acid (**6**), followed by iodination. Subsequently, anthranilic acid derivatives (**9a-9e**) were synthesized using a Ullmann cross-coupling reaction between compound **7** and substituted anilines (**8a-8e**). This reaction utilized potassium carbonate as the base, powdered copper as the catalyst, and ethanol as the solvent, with refluxing for 12 h. Finally, compounds **10a-10e** were obtained through intramolecular acylation of compounds **9a-9e** in concentrated sulfuric acid at 100 °C for three hours (Scheme 1).

All acridone derivatives were obtained in good yields, and their structures were confirmed using NMR and infrared (IR) spectroscopy. The ^{1}H NMR spectra exhibited

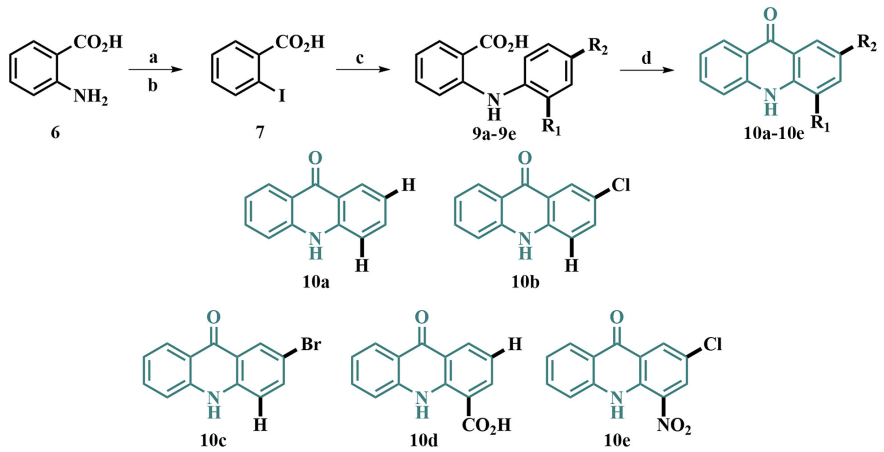

Scheme 1. Synthesis of acridones **10a-10e**. Reagents and conditions (a) $NaNO_{2(aq)}$, HCl, 10 min, 0 °C; (b) $KI_{(aq)}$ 1 h, 0 °C; (c) anilines **8a-8e**, Cu^0, $K_2CO_{3(aq)}$, ethanol, 17 h, reflux; (d) H_2SO_4 3 h, 100 °C.

characteristic signals for the NH proton in the range of 11.16 to 11.96 ppm, while the ^{13}C NMR spectra showed signals corresponding to the carbonyl groups between 175.8 and 177.2 ppm. Additionally, other signals were consistent with the aromatic groups of the acridone scaffold. In IR spectra, characteristic peaks were observed, indicating the presence of functional groups within the acridone structure: N–H stretching (3110-3444 cm^{-1}), aromatic C–H stretching (2972-3086 cm^{-1}), and C=O stretching of carbonyl groups (1618-1710 cm^{-1}). These spectral features corroborate the NMR data, confirming the structures of the synthesized acridones.

Chl a fluorescence measurement

To evaluate the impact of compounds **10a-10e** on the overall performance of PSII, we utilized performance index parameters: on an absorption basis (PI_{ABS}), on the initial cross-section (PI_{CS0}), on the final cross-section (PI_{CSM}), and the total performance index on an absorption basis (PI_{Total}). These parameters were assessed in *S. oleracea* leaf discs exposed to acridone derivatives (Figure 2).

Among the evaluated acridone derivatives, compounds **10a** and **10e** exhibited the most significant inhibitory activities, reducing the PI_{ABS} parameter by

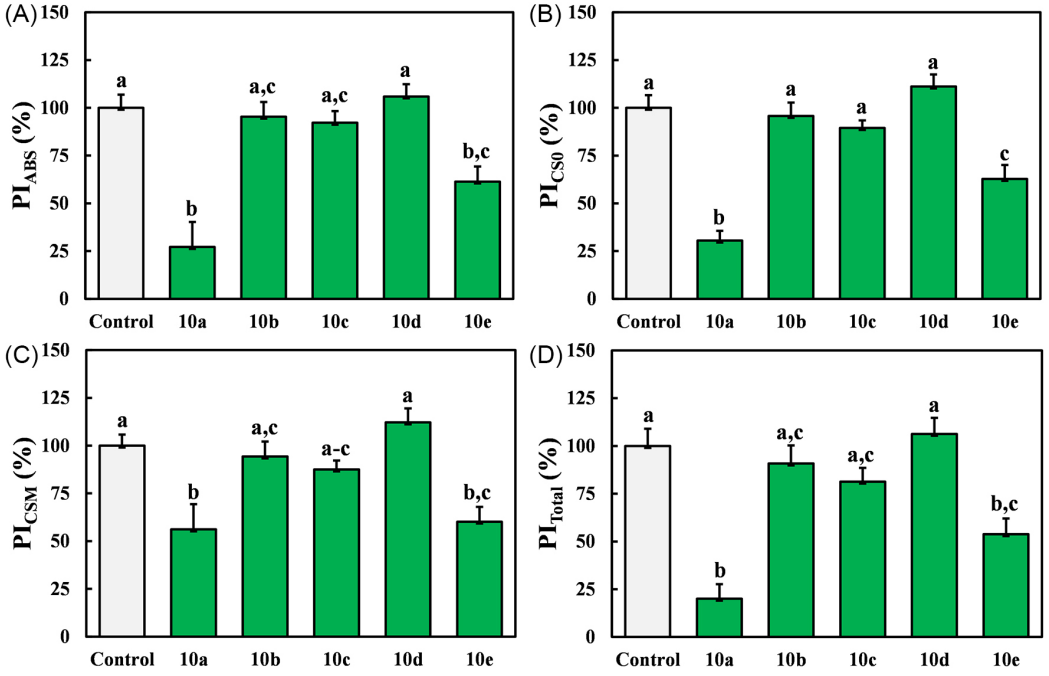

Figure 2. Performance indices of PSII: PI_{ABS} (A), PI_{CS0} (B), PI_{CSM} (C), and PI_{Total} (D) in *S. oleracea* leaf discs treated with compounds **10a-10e** at 100 µM. Aqueous solutions with 1% DMSO was used as control. Values are expressed as mean ± SEM (n = 30). Columns labeled with different letters indicate statistically significant differences ($p < 0.05$).

73 and 39%, respectively (Figure 2A). This reduction indicates a diminished efficiency in the conservation of photon energy absorbed by the PSII for the reduction of electron acceptors.[47] Additionally, compounds **10a** and **10e** decreased the PI_{CS0} parameter by 69 and 37% (Figure 2B), and the PI_{CSM} parameter by 44 and 40% (Figure 2C), respectively. This indicates a reduction in electron transport chain and potential degradation of the protein D1.[48] Furthermore, compounds **10a** and **10e** led to a reduction in the PI_{Total} parameter by 80 and 46% (Figure 2D), respectively, indicating to a decreased energy conservation capacity within the overall functional activity of PSII, photosystem I, and the intersystem electron transport chain.[49]

The observed effects of compounds **10a** and **10e** on the flux ratio parameters absorbance *per* reaction center (ABS/RC) and maximum trapping rate *per* reaction center (TR_0/RC) (Figure 3) suggest that these compounds do not affect the absorption and trapping processes within the photosynthetic reaction centers. However, both compounds decreased the electron transport flux *per* active reaction center (ET_0/RC) by 26 and 23%, respectively (Figure 3). This reduction implies an impairment in electron transfer efficiency within the photosynthetic reaction centers, potentially disrupting electron transport chain and reducing overall photosynthetic efficiency and energy production.[50] Moreover, compounds **10a** and **10e** increased the dissipated energy flux *per* reaction center (DI_0/RC) parameter by 23 and 17% (Figure 3), respectively. This increase indicates a greater loss of absorbed energy through non-photochemical processes, such as heat dissipation and fluorescence emission, as well as energy transfer to non-photosynthetic systems.[51]

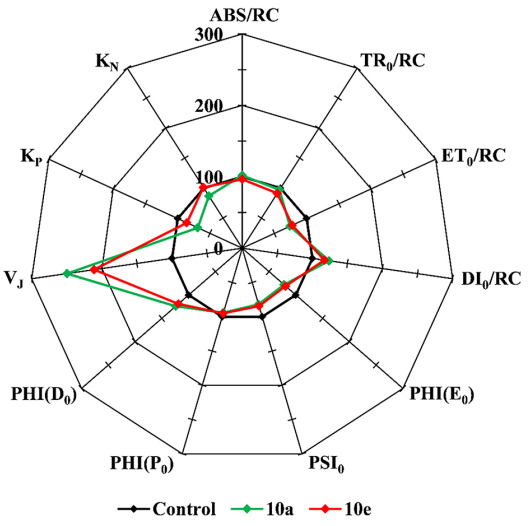

Figure 3. Radar plot of Chl a fluorescence parameters measured in foliar discs of *S. oleracea* after treatment with compounds **10a-10e** at 100 μM. Aqueous solutions with 1% DMSO was used as control. The values are expressed as mean (n = 30).

The observed reductions in the quantum yield for electron transport ($PHI(E_0)$) by 22 and 19% for compounds **10a** and **10e**, respectively (Figure 3), suggest a decrease in the effective quantum yield of PSII electron transport in the presence of photochemical quenching, indicating potential alterations in the efficiency of electron transfer processes within PSII.[52] Additionally, the decreases in the quantum yield of electron transport *per* trapped excitation (PSI_0) by 19 and 16% for compounds **10a** and **10e**, respectively (Figure 3), imply a reduction in the quantum yield of PSII photochemistry under conditions of photochemical quenching, indicating a potential impairment in the ability of PSIIs to utilize absorbed light energy for photochemical reactions.[53] Furthermore, the reductions in the maximal quantum yield of PSII ($PHI(P_0)$) by 6 and 5% for compounds **10a** and **10e**, respectively (Figure 3), indicate a decline in the maximum quantum yield of PSII photochemistry in the absence of photochemical quenching, suggesting potential alterations in the functional integrity of PSII under these conditions.[54]

Compounds **10a** and **10e** demonstrated effects on the quantum yield for energy dissipation ($PHI(D_0)$), with compound **10a** showing a higher increase of 24% compared to 19% for compound **10e** (Figure 3). This increase suggests an enhancement in the quantum yield of non-photochemical energy dissipation processes within PSII, which may indicate adaptive mechanisms to mitigate the impact of excess absorbed light energy and protect PSII from photodamage.[55] These findings are similar to those reported for natural acridone derivatives such as Citrusinine-I, obtained from *Swinglea glutinosa*. Citrusinine-I is known to inhibit the electron transport chain by targeting key sites of the D1 protein.[2] The synthetic acridones studied here, particularly compounds **10a** and **10e**, demonstrated analogous effects, including reductions of $PHI(E_0)$ and PSI_0 parameters, and an increase in the $PHI(D_0)$ parameter. This suggests that these synthetic derivatives share a similar mechanism of action with natural acridones, reinforcing their potential as PSII inhibitors by disrupting electron transport processes and increasing non-photochemical energy dissipation to protect against photodamage.

Additionally, compounds **10a** and **10e** significantly influenced the relative variable fluorescence at *J*-step (V_J), increasing it by 150 and 111%, respectively, compared to the control (Figure 3).[56] The V_J parameter, which reflects the amplitude of the *J*-step, indicates the size of the plastoquinone (PQ) pool and the efficiency of electron transport beyond PSII. The observed increase in V_J suggests modifications in the photosynthetic machinery, potentially reflecting changes in PSII efficiency, electron transport rates, or the redox state of the PQ pool.[57]

Furthermore, both compounds impacted the rate constants for photochemical (K_P) and non-photochemical (K_N) processes. Specifically, compound **10a** reduced the K_P parameter by 32%, while compound **10e** exhibited a smaller reduction of 15% (Figure 3). The K_P parameter is linked to the efficiency of electron transfer from the primary quinone acceptor (Q_A) to the PQ pool. The observed reductions suggest that these compounds may interfere with electron transfer efficiency, potentially by altering the redox state of Q_A.[58] Additionally, compound **10a** decreased the K_N parameter by 13% (Figure 3). The K_N parameter is associated with non-photochemical de-excitation processes, including thermal dissipation and fluorescence emission. The reduction in K_N suggests that compound **10a** may affect the efficiency or capacity of dissipative mechanisms, such as thermal dissipation or the energy transfer to other molecules.

Pre- and post-emergence assay

The phytotoxic activity of acridone derivatives **10a-10e** on the germination, radicle, and hypocotyl growth of *Amaranthus* species was evaluated at a concentration of 100 μM. The results indicate that, at this concentration, compounds **10a-10e** did not significantly affect the overall GP parameter of *A. lividus* seeds (Figure 4A), suggesting that these compounds did not influence the proportion of seeds that successfully germinated under the experimental conditions. However, compounds **10b**-**10c** and **10e** reduced the GI parameter by 16, 16, and 12%, respectively (Figure 4B). The GI parameter reflects the speed and uniformity of seed germination, and the observed decreases imply that these compounds may have inhibited or delayed the germination process, resulting in a slower and less uniform germination compared to the control.

Furthermore, compounds **10b** and **10c** led to increases in the MGT parameter by 19 and 18%, respectively (Figure 4C). This indicates that these compounds prolonged the time required for seeds to germinate, suggesting a delay in seedling emergence under their influence. Overall, these findings imply that compounds **10b**, **10c**, and **10e** exhibit potential inhibitory effects on the germination process of *A. lividus* seeds, affecting both the speed and uniformity of germination.

Compound **10b** caused a reduction in HL parameter by 24% in *A. lividus* seedlings, indicating its ability to inhibit hypocotyl elongation post-germination (Figure 4D). A similar reduction in HL parameter was observed with compound **10a**, which decreased HL parameter by 26% compared to control. Additionally, compound **10b** reduced the RL parameter by 72% compared to the control (Figure 4E), indicating an inhibitory effect on radicle elongation post-germination. Treatment with compounds **10a-10e** led to a reduction in the SVI of *A. lividus* plants, with an average decrease ranging from 35 to 67% (Figure 4F).

The significant decrease in the SVI parameter indicates that the application of acridone derivatives impaired seedling development, affecting the ability of weed seeds to produce normal seedlings. Overall, compounds **10b**-**10c**

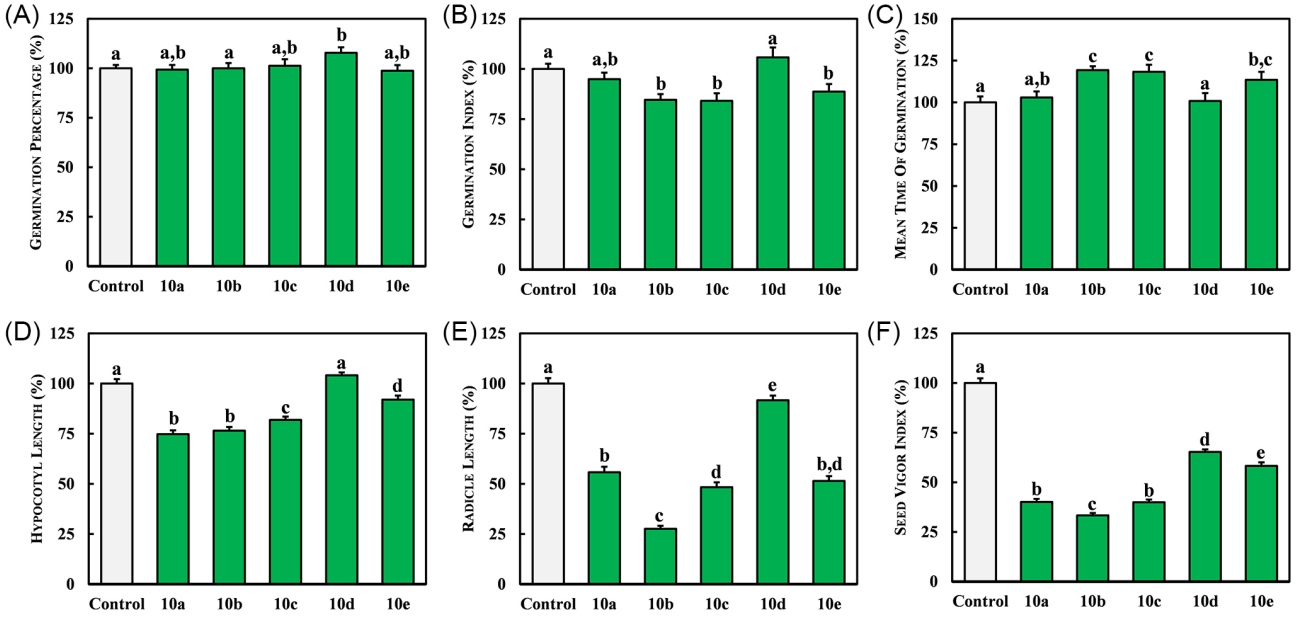

Figure 4. Effects of acridone derivatives **10a-10e** on the parameters: GP (A), GI (B), MGT (C), HL (D), RL (E), and SVI (F) of *A. viridis* weed. Aqueous solutions with 1% DMSO was used as control. Values are expressed as mean ± SEM (n = 175). Columns with different letters are significantly different ($p < 0.05$) from each other.

and **10e** demonstrated promising effects in suppressing the growth of *A. lividus* seedlings post-emergence, particularly by inhibiting hypocotyl and radicle elongation. These findings suggest their potential utility as inhibitors of seedling growth in this species.

In contrast, compounds **10a-10e** did not significantly impact the parameters: GP (Figure 5A), GI (Figure 5B), and MGT (Figure 5C) of *A. viridis* seeds compared to control, except for compound **10d**, which increased the GP parameter by 50%. In post-emergence analysis, compounds **10a** and **10d** showed promising results. Although compound **10d** increased GP parameter, it reduced HL parameter by 26% (Figure 5D), suggesting an inhibitory effect on hypocotyl elongation after seedling emergence. Additionally, compounds **10a** and **10b** reduced HL parameters by an average of 21% compared to the control (Figure 5D). Compound **10d** also decreased RL parameter by 35% compared to the control (Figure 5E), indicating an inhibitory effect on radicle elongation post-germination.

Acridones **10c** and **10d** reduced SVI parameter of *A. viridis* by 35 and 30%, respectively (Figure 5F), indicating a decline in overall seedling vigor. Based on seed germination and seedling growth parameters, key indicators for assessing seed production capacity, the acridone derivatives demonstrated potential pre- and post-emergence herbicidal activity against *Amaranthus weeds*.

The synthetized acridones exhibited comparable or superior phytotoxic activity to other acridone alkaloids reported in the literature for weed growth inhibition. For example, in phytotoxicity studies involving *Lepidium sativum*, *Lactuca sativa*, *Lycopersicon esculentum*, and *Allium cepa*, the acridone graveoline at 1 mM showed significant effects on *L. sativum*, reducing GP and HL parameters by 83 and 75%, respectively.[6] Based on these data, the synthetic acridone derivatives emerge as a promising chemical class for weed control. Specifically, compounds **10a** and **10b** exhibited inhibitory effects on HL parameters in *A. lividus*, while compound **10d** showed similar inhibitory effects on *A. viridis*. These findings indicate that these synthetic acridone derivatives can significantly impair the growth and development of these weed seedlings, highlighting their potential utility as herbicidal agents.

Molecular docking

Molecular docking studies of acridone derivatives **10a-10e** were conducted to understand their potential mechanisms underlying photosynthetic and plant growth inhibitory activities. These compounds were docked against two key protein targets: the D1 protein, a crucial component of PSII, and the enzyme HPPD. Table 1 summarizes the docking results, detailing the binding energies and key intermolecular interactions with both the D1 protein and the HPPD enzyme.

The D1 protein, also known as PsbA, is a crucial component of PSII, a protein complex located in the thylakoid membrane of chloroplasts in plants and cyanobacteria. This protein plays a central role in photosynthesis by capturing

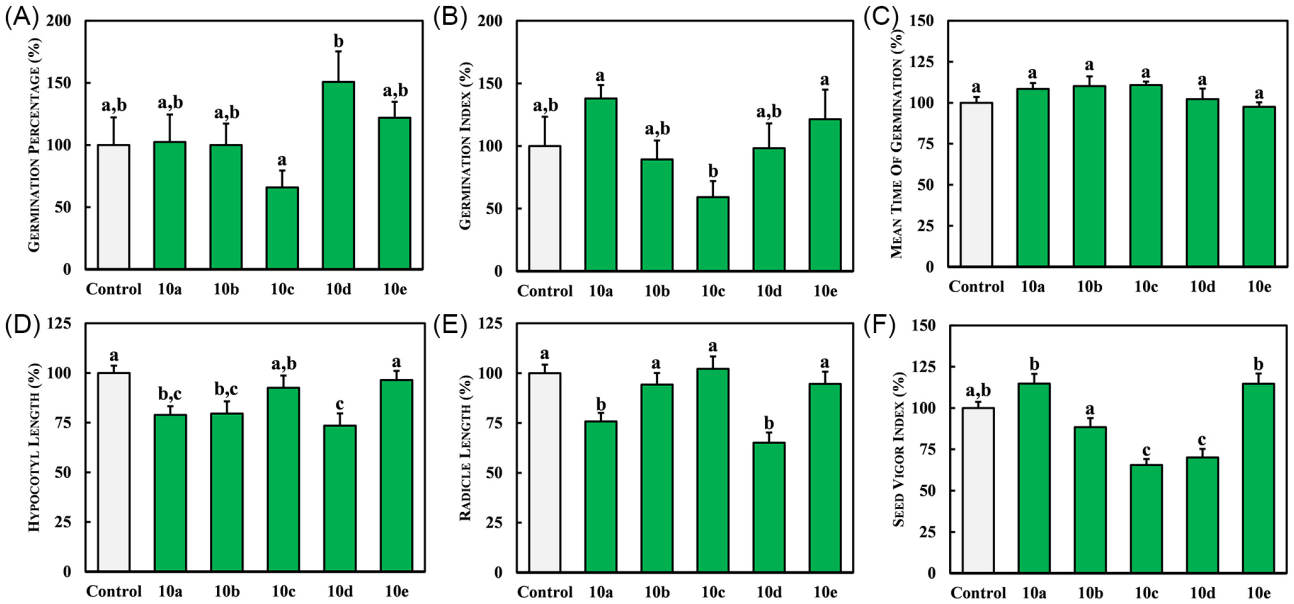

Figure 5. Effects of acridone derivatives **10a-10e** on the parameters: GP (A), GI (B), MGT (C), HL (D), RL (E), and SVI (F) of *A. lividus* weed. Aqueous solutions with 1% DMSO was used as control. Values are expressed as mean ± SEM (n = 175). Columns with different letters are significantly different ($p < 0.05$) from each other.

Table 1. Molecular docking results of compounds **10a-10e**

Compound	Target protein	Binding energy / (kcal mol^{-1})	Key interacting residues
10a	D1 protein	–9.20	Phe265
	HPPD	–7.60	Phe419
10b	D1 protein	–9.10	Phe265
	HPPD	–7.90	–
10c	D1 protein	–8.50	Phe265
	HPPD	–7.90	–
10d	D1 protein	–8.90	Phe265 and His215
	HPPD	–8.60	Asn282, Phe419 Gln379
10e	D1 protein	–9.30	Phe265 and His215
	HPPD	–8.20	Gln307

HPPD: 4-hydroxyphenylpyruvate dioxygenase.

light energy and initiating the electron transport chain. Inhibition of electron flow associated with the D1 protein results in an imbalance between the rates of light absorption and the capacity to utilize this energy in the photosynthetic electron transport chain.[59]

Among the synthesized acridones, compound **10e** demonstrated the highest binding affinity, with a binding energy of –9.30 kcal mol^{-1}. Compound **10e** formed two key hydrogen bonds: one between the nitro group and the Phe265 residue (2.67 Å), and another between its carbonyl group and His215 residue (2.16 Å) (Figure 6a). Additionally, several hydrophobic interactions were observed between compound **10e** and the D1 protein, including π-sigma interactions with Leu118 and Leu271, as well as a π-π stacking interaction with Phe265. These interactions suggest that compound **10e** may effectively inhibit the D1 protein, thereby disrupting photosynthetic electron transport.

Similarly, compound **10a** was docked to elucidate its potential inhibitory activity on photosynthesis. It exhibited a binding energy of –9.20 kcal mol^{-1}, indicating a strong affinity for the D1 protein. Compound **10a** formed a strong hydrogen bond interaction between its carboxyl groups and Phe265 residue (Figure 6b). The acridone scaffold of compound **10a** occupied a hydrophobic binding cleft surrounded by several residues, including Phe211, Met214, Leu218, Phe255, Leu271, Leu275, and Phe274. Hydrophobic interactions were particularly observed between the aromatic ring of compound **10a** and the Met214 and Leu218 residues. Additionally, a π-π interaction was established between Phe265 and the acridone scaffold. Upon comparing the binding poses of compounds **10a** and **10e** with terbutryn, it was observed that the carbonyl group of these acridones occupied a position similar to that of the nitrogen at position 1 of the atrazine scaffold (Figure 6c). This alignment facilitates the formation of a strong hydrogen bond with the NH group of the Phe265 residue, which is crucial for the binding affinity and inhibitory activity of these compounds on the D1 protein of PSII.

HPPD is an enzyme involved in the catabolic pathway of the amino acid phenylalanine and in the biosynthesis of plastoquinone, an essential component of the photosynthetic electron transport chain in plants. Inhibition of HPPD can significantly disrupt plant physiology and growth by affecting these metabolic pathways, leading to a deficiency in plastoquinone and thereby impairing photosynthesis.[22] In the HPPD molecular docking studies, the most active acridones, compounds **10d** and **10e**, demonstrated binding energies of –8.60 and –8.20 kcal mol^{-1}, respectively, indicating strong interactions with the enzyme and suggesting effective of its activity. Detailed analysis of the molecular pose of compound **10d** revealed a hydrogen bond between the backbone NH of Asn282 and the carbonyl group of the acridone scaffold, with hydrogen-bonding distance of 2.19 Å (Figure 7a). Additionally, hydrogen bond interactions were observed between the carboxylic acid group of compound **10d** and the Phe419 and Gln379 residues, with bond distances of 2.45 and 2.07 Å, respectively. This binding orientation positioned the acridone scaffold near the site occupied by the known inhibitor NTBC (Figure 7b), suggesting a similar mode of action in inhibiting HPPD activity.

Acridone **10e** forms a strong hydrogen bond between its nitro group and the NH_2 group of Gln307 residue, with a bond

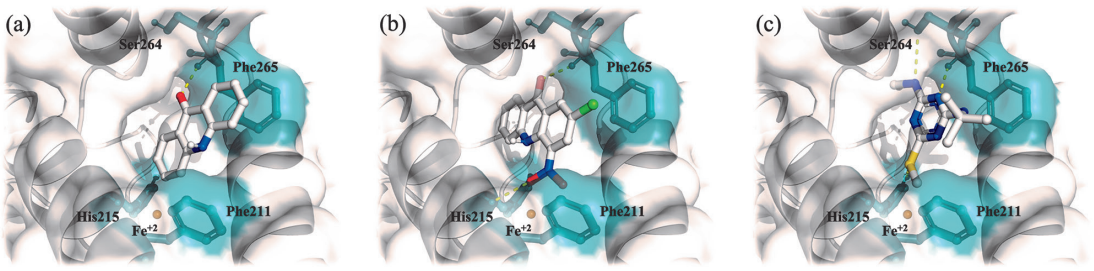

Figure 6. Binding poses of acridone derivatives **10a** (a) and **10e** (b), and terbutryn (c) within the active site of D1 protein of PSII (PDB code: 4V82).

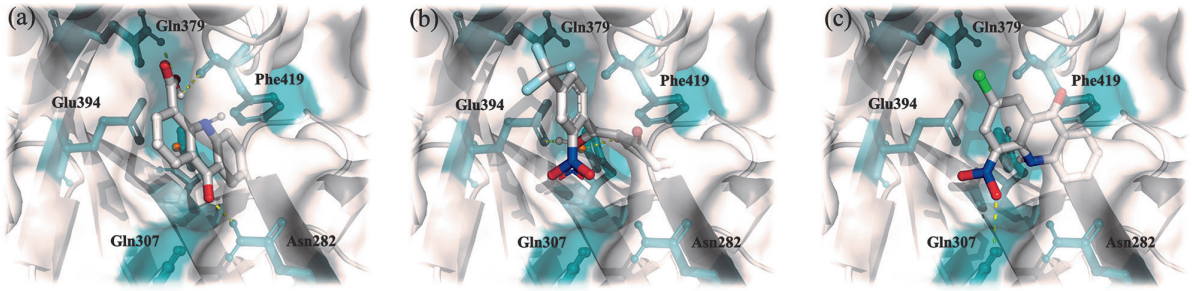

Figure 7. Binding poses of acridone **10d** (a), NTBC (b), and acridone **10e** (c) within the active site of HPPD protein (PDB code: 6J63).

length of 2.86 Å (Figure 7c). Additionally, compound **10e** establishes several hydrophobic contacts with the HPPD protein, including π-alkyl interactions with Val228 and Pro280 residues, as well as a π-π stacking interaction with Phe381 residue. Furthermore, coordination interactions between the Fe^{2+} ion of the heme cofactor and the aromatic rings of compounds **10d** and **10e** were observed, with bond lengths of 3.79 and 4.86 Å, respectively. These interactions contribute to the binding affinity and inhibitory activity of these acridones against the HPPD enzyme, potentially contributing to their phytotoxic effects.

Conclusions

This work demonstrates the synthesis of acridone derivatives using the Ullmann reaction and their evaluation as inhibitors of the PSII electron transport chain and plant growth. The PSII experiments indicated that the most effective acridones were compounds **10a** and **10e**, both of which significantly reduced the Chl a fluorescenceparameters related to performance indices, phenomenological parameters, and quantum yields. Additionally, compounds **10a**, **10b**, and **10d** exhibited promising pre- and post-emergent herbicidal activity by reducing seed germination and seedling growth in germination assays with *Amaranthus* weeds. Molecular docking studies revealed that the acridone derivatives established significant interactions within the binding pockets of the D1 protein of PSII and the HPPD enzyme. These interactions contribute to the observed inhibitory effects on photosynthetic processes and plant growth. Future research will focus on optimizing the structural features of these compounds to enhance their efficacy and to explore their potential as novel herbicide candidates.

Supplementary Information

Supplementary information including spectroscopic data, molecular docking poses, infrared spectra, and ^{1}H and ^{13}C NMR spectra for all synthesized acridone derivatives is available free of charge at http://jbcs.sbq.org.br as PDF file.

Acknowledgments

The authors express their appreciation to CNPq (grant 420048/2023-5) and UFMT for financial support and fellowships. This study was financed in part by the Coordenação de Aperfeiçoamento de Pessoal de Nível Superior - Brasil (CAPES) - Finance Code 001.

Author Contributions

The manuscript was written through contributions of all authors; O. M. S., L. C. C. V. were responsible for study design; J. M. S., P. S. M., T. S. P., L. C. C. V. for synthesis; M. A. S., M. A. F. B., O. M. S. for biological assays; L. G. V., E. L. D., L. C. C. V., O. M. S. for data analysis; P. S. M., L. C. C. V. for molecular docking. All authors contributed to manuscript revision and gave final approval for publication.

References

1. Seifinoferest, B.; Tanbakouchian, A.; Larijani, B.; Mahdavi, M.; *Asian J. Org. Chem.* **2021**, *10*, 1319. [Crossref]
2. dos Santos, D. A. P.; Vieira, P. C.; da Silva, M. F. G. F.; Fernandes, J. B.; Rattray, L.; Croft, S. L.; *J. Braz. Chem. Soc.* **2009**, *20*, 644. [Crossref]
3. Aarjane, M.; Slassi, S.; Amine, A.; *J. Mol. Struct.* **2021**, *1241*, 130636. [Crossref]
4. Chen, H.; Lin, J.; Zhu, S.; Zeng, K.; Tu, P.; Jiang, Y.; *Phytochemistry* **2022**, *203*, 113369. [Crossref]
5. Trinh, D. H.; Tran, P. T.; Trinh, B. T. D.; Nguyen, H. T.; Nguyen, H. D.; Ha, L. D.; Nguyen, L.-H. D.; *Phytochem. Lett.* **2020**, *35*, 94. [Crossref]
6. Nebo, L.; Varela, R. M.; Molinillo, J. M. G.; Sampaio, O. M.; Severino, V. G. P.; Cazal, C. M.; Fernandes, M. F. G.; Fernandes, J. B.; Macías, F. A.; *Phytochem. Lett.* **2014**, *8*, 226. [Crossref]
7. Sverdrup, L. E.; Krogh, P. H.; Nielsen, T.; Kjær, C.; Stenersen, J.; *Chemosphere* **2003**, *53*, 993. [Crossref]
8. Amaral, A. A.; Willig, J. C. M.; Olguin, C. F. A.; Oliveira, I. M.; Stefani, H. A.; Botteselle, G. V.; Manarin, F.; *J. Braz. Chem. Soc.* **2023**, *34*, 1464. [Crossref]
9. Liu, Y.-X.; Zhao, H.-P.; Wang, Z.-W.; Li, Y.-H.; Song, H.-B.;

Riches, H.; Beattie, D.; Gu, Y.-C.; Wang, Q.-M.; *Mol. Diversity* **2013**, *17*, 701. [Crossref]
10. Bermúdez-Torres, K.; Herrera, J. M.; Brito, R. F.; Wink, M.; Legal, L.; *BioControl* **2009**, *54*, 459. [Crossref]
11. Wang, D.-W.; Lin, H.-Y.; Cao, R.-J.; Ming, Z.-Z.; Chen, T.; Hao, G.-F.; Yang, W.-C.; Yang, G.-F.; *Pest Manage. Sci.* **2015**, *71*, 1122. [Crossref]
12. Veiga, T. A. M.; King-Díaz, B.; Marques, A. S. F.; Sampaio, O. M.; Vieira, P. C.; da Silva, M. F. G. F.; Lotina-Hennsen, B.; *J. Photochem. Photobiol., B* **2013**, *120*, 36. [Crossref]
13. Mendes, M. C. D. S.; Fazolo, B. R.; de Souza, J. M.; de Vasconcelos, L. G.; de Sousa Jr., P. T. S.; Dall'Oglio, E. L.; Soares, M. A.; Sampaio, O. M.; Vieira, L. C. C.; *Photochem. Photobiol. Sci.* **2019**, *18*, 1350. [Crossref]
14. Soares, L. T. X. M. G.; Basso, M. A. F.; dos Santos, C. M. R.; Ali, A.; Vasconcelos, L. G.; Dall'Oglio, E. L.; Sampaio, O. M.; Vieira, L. C. C.; *Chem. Biodiversity* **2022**, *19*, e202200586. [Crossref]
15. de Souza, J. M.; Fazolo, B. R.; Lacerda, J. W. F.; Moura, M. S.; Santos, A. C. R.; Vasconcelos, L. G.; de Sousa Jr., P. T. S.; Dall'Oglio, E. L.; Ali, A.; Sampaio, O. M.; Vieira, L. C. C.; *Photochem. Photobiol.* **2020**, *96*, 1233. [Crossref]
16. Sampaio, O. M.; Vieira, L. C. C.; Bellete, B. S.; King-Diaz, B.; Lotina-Hennsen, B.; da Silva, M. F. G. F.; Veiga, T. A. M.; *Molecules* **2018**, *23*, 2693. [Crossref]
17. Ferreira, P. H. A.; dos Santos, D. A. P.; da Silva, M. F. G. F.; Vieira, P. C.; King-Diaz, B.; Lotina-Hennsen, B.; Veiga, T. A. M.; *Chem. Biodiversity* **2016**, *13*, 100. [Crossref]
18. Battaglino, B.; Grinzato, A.; Pagliano, C.; *Plants* **2021**, *10*, 1501. [Crossref]
19. Wang, Y.; Liu, W.; Dong, B.; Wang, D.; Nian, Y.; Zhou, H.; *Plants* **2023**, *12*, 2576. [Crossref]
20. de Pádua, G. M. S.; Pitteri, T. S.; Basso, M. A. F.; de Vasconcelos, L. G.; Ali, A.; Dall'Oglio, E. L.; Sampaio, O. M.; Vieira, L. C. C.; *Chem. Biodiversity* **2024**, *21*, e202301564. [Crossref]
21. Jiang, M.; Yang, Q.; Wang, H.; Luo, Z.; Guo, Y.; Shi, J.; Wang, X.; Qiang, S.; Strasser, R. J.; Chen, S.; *Plants* **2022**, *11*, 2797. [Crossref]
22. Ndikuryayo, F.; Moosavi, B.; Yang, W.-C.; Yang, G.-F.; *J. Agric. Food Chem.* **2017**, *65*, 8523. [Crossref]
23. Fu, Y.; Wang, M.; Zhao, L.-X.; Zhang, S.-Q.; Liu, Y.-X.; Guo, Y.-Y.; Zhang, D.; Gao, S.; Ye, F.; *Pestic. Biochem. Physiol.* **2021**, *174*, 104811. [Crossref]
24. Hu, W.; Gao, S.; Zhao, L.; Guo, K.; Wang, J.; Gao, Y.; Shao, X.; Fu, Y.; Ye, F.; *Pest Manage. Sci.* **2022**, *78*, 938. [Crossref]
25. Fu, Q.; Cai, P.; Cheng, L.; Zhong, L.; Tan, C.; Shen, Z.; Han, L.; Xu, T.; Liu, X.; *Pest Manage. Sci.* **2020**, *76*, 868. [Crossref]
26. Gorlushko, D. A.; Filimonov, V. D.; Krasnokutskaya, E. A.; Semenischeva, N. I.; Go, B. S.; Hwang, H. Y.; Cha, E. H.; Chi, K.-W.; *Tetrahedron Lett.* **2008**, *49*, 1080. [Crossref]
27. Mohammadi-Khanaposhtani, M.; Shabani, M.; Faizi, M.; Aghaei, I.; Jahani, R.; Sharafi, Z.; Shamsaei Zafarghandi, N.; Mahdavi, M.; Akbarzadeh, T.; Emami, S.; Shafiee, A.; Foroumadi, A.; *Eur. J. Med. Chem.* **2016**, *112*, 91. [Crossref]
28. Pintér, Á.; Klussmann, M.; *Adv. Synth. Catal.* **2012**, *354*, 701. [Crossref]
29. Tseng, H.-J.; Lin, M.-H.; Shiao, Y.-J.; Yang, Y.-C.; Chu, J.-C.; Chen, C.-Y.; Chen, Y.-Y.; Lin, T. E.; Su, C.-J.; Pan, S.-L.; Chen, L.-C.; Wang, C.-Y.; Hsu, K.-C.; Huang, W.-J.; *Eur. J. Med. Chem.* **2020**, *192*, 112193. [Crossref]
30. Goodell, J. R.; Puig-Basagoiti, F.; Forshey, B. M.; Shi, P.-Y.; Ferguson, D. M.; *J. Med. Chem.* **2006**, *49*, 2127. [Crossref]
31. Binaschi, M.; Boldetti, A.; Gianni, M.; Maggi, C. A.; Gensini, M.; Bigioni, M.; Parlani, M.; Giolitti, A.; Fratelli, M.; Valli, C.; Terao, M.; Garattini, E.; *ACS Med. Chem. Lett.* **2010**, *1*, 411. [Crossref]
32. Pang, X.; Lou, Z.; Li, M.; Wen, L.; Chen, C.; *Eur. J. Org. Chem.* **2015**, *2015*, 3361. [Crossref]
33. Gopinath, V. S.; Thimmaiah, P.; Thimmaiah, K. N.; *Bioorg. Med. Chem.* **2008**, *16*, 474. [Crossref]
34. Verones, V.; Flouquet, N.; Lecoeur, M.; Lemoine, A.; Farce, A.; Baldeyrou, B.; Mahieu, C.; Wattez, N.; Lansiaux, A.; Goossens, J.-F.; Berthelot, P.; Lebegue, N.; *Eur. J. Med. Chem.* **2013**, *59*, 39. [Crossref]
35. Orlov, V. Y.; Ganzha, V. V.; Kotov, A. D.; Sokolov, V. G.; *Russ. J. Org. Chem.* **2007**, *43*, 1502. [Crossref]
36. Moura, M. S.; Lacerda, J. W. F.; Siqueira, K. A.; Bellete, B. S.; Sousa, P. T.; Dall´Óglio, E. L.; Soares, M. A.; Vieira, L. C. C.; Sampaio, O. M.; *J. Environ. Sci. Health, Part B* **2020**, *55*, 470. [Crossref]
37. Khan, A. M.; Mobli, A.; Werth, J. A.; Chauhan, B. S.; *PLoS One* **2022**, *17*, e0263798. [Crossref]
38. Broser, M.; Glöckner, C.; Gabdulkhakov, A.; Guskov, A.; Buchta, J.; Kern, J.; Müh, F.; Dau, H.; Saenger, W.; Zouni, A.; *J. Biol. Chem.* **2011**, *286*, 15964. [Crossref]
39. Lin, H.-Y.; Yang, J.-F.; Wang, D.-W.; Hao, G.-F.; Dong, J.-Q.; Wang, Y.-X.; Yang, W.-C.; Wu, J.-W.; Zhan, C.-G.; Yang, G.-F.; *FEBS J.* **2019**, *286*, 975. [Crossref]
40. *AutoDockTools*, version 1.5.7; The Scripps Research Institute; USA, 2022.
41. *ChemDraw*, version 19.0; PerkinElmer Informatics, Inc.; CambridgeSoft, USA, 2019.
42. *AutoDock Vina*, version 1.2.5; The Scripps Research Institute, USA, 2024.
43. *AutoDock*, version 4.2.6; The Scripps Research Institute, USA, 2022.
44. *Discovery Studio Visualizer*, version 21.1.0.20298; Biovia, USA, 2012.
45. *The PyMOL Molecular Graphics System*, version 2.1.0; Schrödinger, LLC., USA, 2018.
46. *GraphPad Prism*, version 8.0; GraphPad Software, Inc., USA, 2019.

47. Mihaljević, I.; Vuletić, M. V.; Tomaš, V.; Horvat, D.; Zdunić, Z.; Vuković, D.; *Photosynthetica* **2021**, *59*, 517. [Crossref]
48. Ran, X.; Wang, X.; Gao, X.; Liang, H.; Liu, B.; Huang, X.; *PLoS One* **2021**, *16*, e0260086. [Crossref]
49. Hu, W.; Snider, J. L.; Chastain, D. R.; Slaton, W.; Tishchenko, V.; *Environ. Exp. Bot.* **2018**, *155*, 360. [Crossref]
50. Pan, X.; Deng, C.; Zhang, D.; Wang, J.; Mu, G.; Chen, Y.; *Aquat. Toxicol.* **2008**, *89*, 207. [Crossref]
51. Sharma, J.; Singh, H.; Sharma, S.; Kumar, D.; Bhatt, U.; Soni, V.; *Plant Physiol. Rep.* **2022**, *27*, 603. [Crossref]
52. Xia, J.; Tian, Q.; *J. Environ. Sci.* **2009**, *21*, 1569. [Crossref]
53. Wang, G.; Hao, Z.; Anken, R. H.; Lu, J.; Liu, Y.; *Adv. Space Res.* **2010**, *45*, 839. [Crossref]
54. Xiang, R.; Shi, J.; Zhang, H.; Dong, C.; Liu, L.; Fu, J.; He, X.; Yan, Y.; Wu, Z.; *Aquat. Toxicol.* **2018**, *200*, 188. [Crossref]
55. Orekhova, A.; Barták, M.; Casanova-Katny, A.; Hájek, J.; *Plant Biol.* **2021**, *23*, 653. [Crossref]
56. de Pádua, G. M. S.; de Souza, J. M.; Sales, M. C. M.; de Vasconcelos, L. G.; Dall'Oglio, E. L.; Faraggi, T. M.; Sampaio, O. M.; Vieira, L. C. C.; *Chem. Biodiversity* **2021**, *18*, e2100226. [Crossref]
57. Zhang, D.; Pan, X.; Mu, G.; Wang, J.; *J. Appl. Phycol.* **2010**, *22*, 479. [Crossref]
58. Chen, L. S.; Cheng, L.; *Photosynthetica* **2009**, *47*, 112. [Crossref]
59. Zharmukhamedov, S. K.; Allakhverdiev, S. I.; *Russ. J. Plant Physiol.* **2021**, *68*, 212. [Crossref]

Submitted: September 30, 2024
Published online: December 16, 2024